



ELSEVIER

Available online at www.sciencedirect.com

SCIENCE @ DIRECT®

Earth and Planetary Science Letters 222 (2004) 485–500

EPSL

www.elsevier.com/locate/epsl

The influence of thermochemical convection on the fixity of mantle plumes

Allen K. McNamara*, Shijie Zhong

Department of Physics, University of Colorado, 390 UCB, Boulder, CO 80309-0390, USA

Received 8 August 2003; received in revised form 20 February 2004; accepted 3 March 2004

Abstract

A general feature of both isochemical and thermochemical studies of mantle convection is that horizontal plume velocities tend to be smaller than typical convective velocities, however, it is not clear which system leads to a greater fixity of mantle plumes. We perform two- and three-dimensional numerical calculations and compare both thermochemical and isochemical cases with similar convective vigor to determine whether presence of a dense component in the mantle can lead to smaller ratios of horizontal plume velocity to surface velocity. We investigate different viscosity and density contrasts between chemical components in the thermochemical calculations, and we perform isochemical calculations with both free-slip and no-slip bottom boundary conditions. We then compare both visually and quantitatively the results of the thermochemical and isochemical calculations to determine which leads to greater plume fixity. We find that horizontal plume velocities for thermochemical calculations are similar to those from isochemical calculations with no-slip bottom boundary conditions. In addition, we find that plumes tend to be more fixed for isochemical cases with free-slip bottom boundary conditions for two-dimensional calculations, however, in three dimensions, we find that plume fixity is similar to that observed in thermochemical calculations. © 2004 Elsevier B.V. All rights reserved.

Keywords: plumes; mantle convection; thermochemical convection; lower mantle

1. Introduction

Ocean–island tracks and some continental volcanic sequences are generally considered to have formed by moving tectonic plates over hotspots, which are generally thought to be surface manifestations of deep-rooted mantle plumes originating from a thermal boundary layer in the lower mantle [1]. While there may be approximately 30–100 hotspots observed on

the Earth's surface [2,3], the difficulty of seismically imaging plumes (e.g., [4]) makes this model troublesome to test. However, there is evidence that suggests at least some of these hotspots are derived from a deep mantle origin [5].

Originally, hotspots were hypothesized to be spatially fixed [6], but it was later discovered that they do move. Their velocities relative to each other appear to be an order of magnitude smaller than typical plate velocities (e.g., [7–10]). Richards [11] first suggested that the relative fixity of plumes was related to a high-viscosity lower mantle. In global kinematic mantle flow models with plate motion and passive plumes, Steinberger and O'Connell [12] have shown that the

* Corresponding author. Tel.: +1-303-735-4892; fax: +1-303-492-7935.

E-mail address: mcnamar@colorado.edu (A.K. McNamara).

relative motions of hotspots could be explained with more than two orders increase of viscosity from the upper mantle to the lower mantle. Numerical calculations of isochemical thermal convection in a three-dimensional spherical geometry [13] have revealed that plumes tend to form at stagnation points along the core–mantle boundary, and that the locations and horizontal motion of plumes are primarily controlled by the geometry of down welling material. However, they found horizontal plume motions on average are about one-third of plate velocities for models with lower mantle viscosity that is 60 times that of the upper mantle, suggesting that either a significantly larger viscosity contrast between the lower and upper mantle or other physical mechanisms are needed to reproduce the observed small hotspot motions. Three-dimensional Cartesian calculations with tectonic plates [14] also exhibit relatively fixed plumes for lower to upper mantle viscosity ratios as low as 30, likely resulting from plumes migrating to stagnation points.

The plume model has often been extended to include a more-dense chemical component in the lower mantle (e.g., [15–20]). In this case, plumes may originate from the density interface which may serve to explain the difference in geochemistry observed at hotspots as opposed to mid-oceanic ridge basalts [21]. In addition, there is some support of a different chemical component at the base of the mantle based on seismic evidence [22–28].

Several fluid dynamical laboratory studies have studied the influence that a dense component has on plume behavior. Namiki and Kurita [29] found that the presence of an aluminum block at the bottom of their tank experiment, representing a bulge of material at the base of the mantle, can lead to a stationary source of upwelling if the block is thicker than the lower thermal boundary layer. It is difficult to compare this to a thermochemical system, however, in which the dense material may move in response to mantle flow.

Jellinek and Manga [30] have performed thermochemical laboratory experiments in which they inject a dense less viscous layer into the bottom of the tank. They found that entrainment of the dense material provides long-lived, low-viscosity conduits extending from the density interface to the surface. They also found that the time scale for horizontal

plume motion is much longer than plume rise time. They suggested that the presence of a dense layer may provide a mechanism to fix the position of hotspots.

Davaille and co-workers [20,31,32] have performed numerous thermochemical lab studies in which they identify two thermochemical flow regimes based on the deformation of the interface between a dense and less dense component: a stratified regime and a doming one. They suggest that the Earth may presently be in the doming regime, possibly explaining the presence of superplumes (e.g., [33]). They find that long-lived thermochemical plumes may originate from the peaks of the domes. They also find that the thermochemical plumes tend to have horizontal drift velocities much smaller than typical convective velocities. These plumes appear to be “anchored” to the dense layer, but they state that any motions imposed upon the dense layer may cause lateral motion of the “anchor points” at which the plumes are fixed. Examples could include lateral motions imposed by subducting slabs or the rising of domes.

The focus of this work is to distinguish whether the presence of a dense thermochemical component in the Earth’s lower mantle can actually stabilize the location of plume formation. In particular, we investigate whether these plumes are more stationary than those generated in an isochemical convecting system. While laboratory studies have shown that thermochemical systems may produce plumes with horizontal velocities much smaller than convective velocities, it is important to actually compare to isochemical systems of similar vigor in order to determine whether the presence of a dense component can enhance the fixity of plumes. This is essential to concluding whether a dense component is required to satisfy geological constraints of plume fixity. Laboratory studies have shown that plumes tend to be fixed to upwelling points along the interface between dense and less dense components. Given that may be the case, we are essentially investigating the mobility of this interface and the resulting effect on horizontal plume velocity.

We perform a series of thermochemical calculations for two sets of Rayleigh number, multiple values of chemical buoyancy, and different viscosity contrasts between dense and less dense components. We measure the fixity of plumes by determining the ratio

of horizontal plume velocity near its interface of origin to average surface velocities. This ratio is more useful than looking at horizontal plume velocities alone because it provides a measure of how plume velocities relate to plate velocities. We compare each set of thermochemical calculations to isochemical calculations with a Rayleigh number equivalent to the effective Rayleigh number of the top layer of the thermochemical calculation to determine which will provide greater plume fixity. The majority of calculations are performed in two dimensions, however, four calculations (two thermochemical and two isochemical) are repeated using a three-dimensional geometry.

Our results indicate that the presence of a dense component does not promote the fixity of plumes any more than isochemical convection with no-slip bottom boundary conditions. Furthermore, in the two-dimensional cases, equivalent isochemical convection calculations with free-slip bottom boundary conditions generate plumes which appear more stable than those in thermochemical calculations. This final observation is not shown in the three-dimensional calculations, where isochemical and thermochemical plume fixities are similar.

2. Model setup

2.1. Governing equations

The numerical calculations are performed by solving the non-dimensional conservation equations of mass, momentum, and energy in the Boussinesq approximation.

The equation for mass conservation in incompressible flow is:

$$\nabla \cdot \mathbf{u} = 0, \quad (1)$$

where \mathbf{u} is the velocity vector. The momentum equation is:

$$-\nabla P + \nabla \cdot (\eta \underline{\underline{\dot{\epsilon}}}) = (RaT - RbC)\hat{\mathbf{z}}, \quad (2)$$

where $\hat{\mathbf{z}}$ is the vertical unit vector, P is the dynamic pressure, η is the viscosity, $\underline{\underline{\dot{\epsilon}}}$ is the deviatoric strain

rate tensor, T is the temperature, C is the composition, and Ra is the thermal Rayleigh number defined as:

$$Ra = \frac{\alpha \rho g \Delta T h^3}{\eta \kappa}, \quad (3)$$

where α is the thermal expansivity, ρ is the density, g is the acceleration of gravity, ΔT is the temperature drop across the mantle, h is the mantle thickness, and κ is the thermal diffusivity.

Rb is the chemical Rayleigh number defined as:

$$Rb = \frac{\Delta \rho g h^3}{\eta \kappa}, \quad (4)$$

where $\Delta \rho$ is the density contrast between chemical components.

A useful non-dimensional quantity is the buoyancy number, B , which is the ratio of chemical to thermal buoyancy:

$$B = \frac{Rb}{Ra} = \frac{\Delta \rho}{\rho \alpha \Delta T}. \quad (5)$$

The energy equation without internal heating is expressed as:

$$\frac{\partial T}{\partial t} + (\mathbf{u} \cdot \nabla)T = \nabla^2 T, \quad (6)$$

where t is time.

The equation for chemical advection is:

$$\frac{\partial C}{\partial t} + (\mathbf{u} \cdot \nabla)C = 0. \quad (7)$$

2.2. Computational method

The convection equations are solved using the finite element code Citcom [13,35]. The evolution of composition is tracked using tracer particles. Tracers have an advantage over field-based methods in which numerical diffusion is a problem and over marker chain methods which become computationally expensive for complicated flows [34]. We use the ratio tracer method (described and tested in [36]) which utilizes two sets of tracers, representing each component. Tracer particles are advected using a simple predictor–corrector scheme (e.g., [37]), and the composition of each element is determined by

calculating the ratio of dense tracers to all tracers in a given element. Initially, 16 and 10 tracers are placed in each element for the 2-D and 3-D calculations, respectively.

The model geometry for the two-dimensional calculations is a Cartesian box of aspect ratio 6. The velocity boundary conditions are free-slip on the top and side boundaries of all calculations. The thermochemical calculations have free-slip bottom boundary conditions whereas the isochemical calculations employ both free-slip and no-slip bottom velocity boundary conditions for reasons explained below.

The thermochemical calculations are performed on a mesh with 80 vertical and 480 horizontal rectangular elements with grid refinement in the bottom fifth of the box. The isochemical calculations are performed on a mesh with 64 and 384 elements in the vertical and horizontal dimensions, respectively. The thermochemical and isochemical calculations are carried out for 20,000 and 40,000 time steps, respectively. Each calculation has been carried out for times far removed from the initial condition (typically 30–60 transit times).

The three-dimensional thermochemical calculations are performed in $2 \times 2 \times 1$ boxes. We found that isochemical calculations with this aspect ratio produce plumes which quickly migrate to the edges, so boxes with size $3 \times 3 \times 1$ are used for the isochemical calculations.

The thermochemical 3-D calculations employ 81 elements vertically and 129 elements horizontally, and the isochemical calculations have 65 and 161 elements in these directions, respectively. The thermochemical calculations are carried out for times after that in which the dense layer is fully entrained, and the isochemical calculations are carried out for times longer than this.

We investigate lateral plume velocities along a horizontal line (plane for 3-D) at a vertical non-dimensional distance of 0.1 above the interface. This line/plane will be referred as the plume line/plane. The interface is the bottom boundary for the isochemical cases and the average contact depth between the dense and less dense components for thermochemical cases. We determine relative horizontal plume velocities with two different methods. First, qualitatively, we generate plots of temperature along the plume line/plane versus time. This type of representation has been used in [19] and provides a useful measure in a relative sense when comparing calculations of similar convective vigor. Second, quantitatively, we integrate the horizontal velocities along the plume line/plane, filtered by including only nodes which have a residual temperature exceeding a given threshold temperature. We then integrate over approximately 12 transit times and divide by the average surface velocity, $\langle v_{\text{top}} \rangle$, to determine the plume velocity ratio:

$$\frac{1}{\langle v_{\text{top}} \rangle} \frac{1}{L_f \cdot 12\tau} \int_{t=t_f-12\tau}^{t=t_f} \int_{x=0}^{x=L} F(T_r) |V_H| dx dt \quad (8)$$

where

$$F = \begin{cases} 0 & : T_r < T_{\text{th}} \\ 1 & : T_r \geq T_{\text{th}} \end{cases} \quad (9)$$

where L_f is the length along the plume line with temperatures exceeding T_{th} , τ is the transit time defined by the depth of the model divided by the average surface velocity, t_f is the final time, T_r is the residual temperature, V_H is the horizontal velocity, and T_{th} is

Table 1
Sets of thermochemical calculations

Rayleigh number	Viscosity of top layer	Viscosity of bottom layer	Range of B numbers	Estimated ΔT of top layer	Effective Rayleigh number of top layer
5×10^6	1.0	1.0	0.8–1.6	0.5	1.8×10^6
5×10^6	1.0	25.0	0.7–1.0	0.4	1.5×10^6
5×10^6	1.0	0.04	0.9–1.2	0.7	2.6×10^6
10^7 *	1.0	1.0	0.8–1.6	0.5	3.6×10^6
10^7	1.0	25.0	0.7–1.0	0.4	2.9×10^6
10^7 *	1.0	0.04	0.8–1.2	0.7	5.1×10^6

* Indicates where 3-D calculations were also performed ($B=0.8$ for the isoviscous case and $B=0.9$ for the weak dense layer case).

Table 2
Isochemical rescaling

Ra	t_{dim}	t''	q_{dim}	q''	T_{dim}	T''	v_{dim}	v''
1.8×10^6	$(0.9h)^2/\kappa$	$0.81t'$	$k(0.5\Delta T)/(0.9h)$	$0.556q'$	$0.5\Delta T$	$0.5T'$	$\kappa/(0.9h)$	$1.11v'$
1.5×10^6	$(0.9h)^2/\kappa$	$0.81t'$	$k(0.4\Delta T)/(0.9h)$	$0.444q'$	$0.4\Delta T$	$0.4T'$	$\kappa/(0.9h)$	$1.11v'$
2.6×10^6	$(0.9h)^2/\kappa$	$0.81t'$	$k(0.7\Delta T)/(0.9h)$	$0.778q'$	$0.7\Delta T$	$0.7T'$	$\kappa/(0.9h)$	$1.11v'$
3.6×10^6	$(0.9h)^2/\kappa$	$0.81t'$	$k(0.5\Delta T)/(0.9h)$	$0.556q'$	$0.5\Delta T$	$0.5T'$	$\kappa/(0.9h)$	$1.11v'$
2.9×10^6	$(0.9h)^2/\kappa$	$0.81t'$	$k(0.4\Delta T)/(0.9h)$	$0.444q'$	$0.4\Delta T$	$0.4T'$	$\kappa/(0.9h)$	$1.11v'$
5.1×10^6	$(0.9h)^2/\kappa$	$0.81t'$	$k(0.7\Delta T)/(0.9h)$	$0.778q'$	$0.7\Delta T$	$0.7T'$	$\kappa/(0.9h)$	$1.11v'$

Where the subscript dim represents dimensional values of time, t , heat flow, q , temperature, T , and velocity, v for isochemical cases. Primed quantities are non-dimensional values from the isochemical case, and double primed quantities are those rescaled to match the same non-dimensional units as the thermochemical cases. κ and k are thermal diffusivity and conductivity, respectively. ΔT and h are the temperature drop and thickness across the entire mantle for thermochemical models.

the threshold residual temperature. In this study, we define the threshold residual temperature as 0.1.

We concentrate on comparing plume velocities using the more qualitative temperature versus time plots, however, because it is not possible to show all our results in this visible fashion, we also present the integrated plume velocity ratios for all calculations.

We note that the exact numerical value derived from the quantitative method described above is dependent upon the threshold temperature chosen, the height of the plume line, and the number of transit times integrated over. We have found, however, that this method provides the best measure to compare the fixity of plumes between calculations.

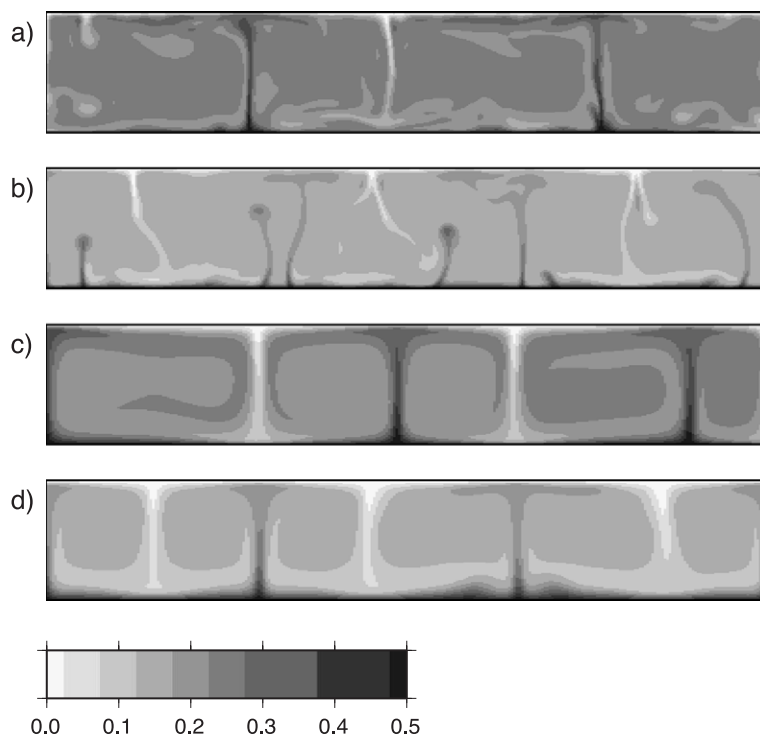


Fig. 1. Snapshots of the temperature fields of four isochemical calculations. The effective Rayleigh numbers are 3.6×10^6 and 3.6×10^5 for (a,b) and (c,d), respectively; (a,c) have free-slip bottom boundary conditions and (b,d) have no-slip bottom boundary conditions. The temperature scale is given at the bottom.

2.3. Thermochemical calculations

We perform thermochemical calculations for two Rayleigh numbers (5×10^6 and 10^7) and three different viscosity contrasts between chemical components (both the same, dense material 25 times more viscous, and dense material 25 times less viscous). The intrinsic viscosity of each component is constant, however. For each set of Rayleigh number and viscosity contrast, we perform thermochemical calculations for several density contrasts (buoyancy numbers). The density contrasts span buoyancy numbers that range from those leading to complete overturn to those leading to completely stratified layers. For this study, we are not interested in results that lead to immediate overturn or rapid mixing. In all cases, the initial thickness of the dense layer is one tenth the mantle thickness.

We estimate the effective Rayleigh number of the top layer for each set of thermochemical calculations,

where a set is defined as a particular combination of input Rayleigh number and viscosity contrast.

$$Ra_{eff} = Ra \frac{\Delta T_{top}}{\Delta T} \left(\frac{h_{top}}{h} \right)^3$$

where ΔT_{top} is the average temperature drop across the top layer estimated as twice the average interior temperature in the top layer. h_{top} is simply the average thickness of the top layer (0.9 in these calculations).

Table 1 lists the properties of each set of calculations.

2.4. Isochemical calculations

For each set of thermochemical calculations, we perform two isochemical calculations with Rayleigh numbers chosen to match that of the effective Rayleigh number of the top layer of that set of thermochemical calculations. This is to ensure that we are comparing isochemical and thermochemical calcula-

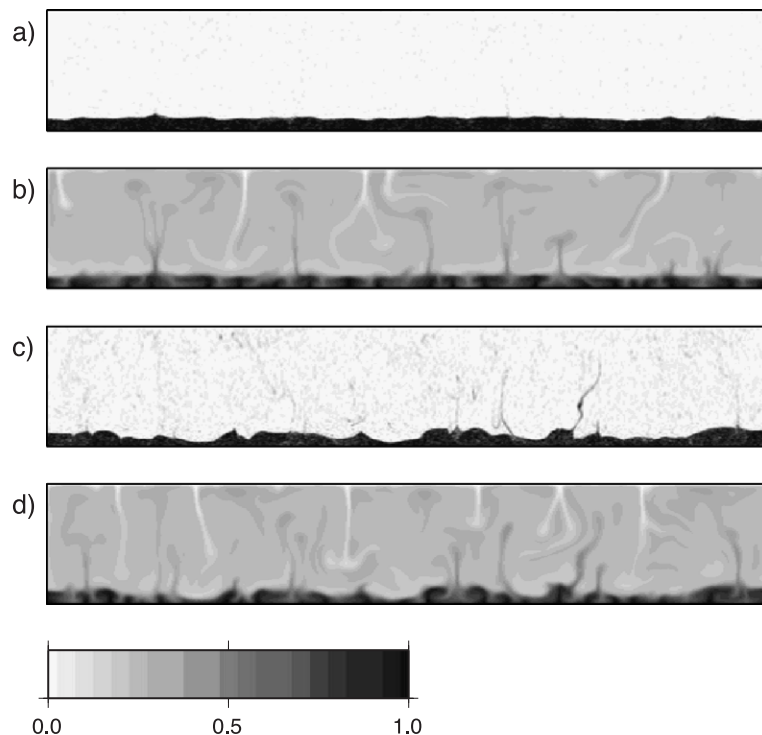


Fig. 2. Compositional (a,c) and temperature (b,d) fields for two thermochemical calculations with an effective Rayleigh number of 3.6×10^6 in their upper layers. The viscosity of both components is equivalent. Buoyancy numbers are 1.4 and 0.8 for (a,b) and (c,d), respectively. Both temperature and composition use the same scale shown at the bottom.

tions of similar vigor. Because the bottom boundary of the top layer in the thermochemical calculations is expected to be partial slip due to viscous coupling between components, we perform isochemical calculations with both no-slip and free-slip bottom boundary conditions for better comparison.

In order to maintain the same non-dimensional units between both sets of calculations, we scale the output values of the isochemical cases to have the same non-dimensional units as the thermochemical calculations. This allows for adequate comparison between both models. The rescaling is done by first dimensionalizing the quantities of time, temperature, heat flow, and velocity of the isochemical cases and then non-dimensionalizing them by the scale factors used in the thermochemical cases. The temperature drop and thickness associated with the thermochemical cases are ΔT and h , respectively. The temperature

drop of the isochemical cases is some fraction of ΔT (given in Table 1) and $0.9h$. Scaling of the isochemical quantities is shown in Table 2.

3. Results

We first present snapshots of the temperature field of four isochemical calculations (Fig. 1). The calculations shown are of two Rayleigh numbers, with free-slip and no-slip bottom boundary conditions. Note that the maximum temperature is 0.5 in accordance to the scaling described previously. One common feature noticed when comparing cases with no-slip and free-slip bottom boundary conditions of the same Rayleigh number is that plume locations are relatively more stable and the overall vigor of convection is greater in the free-slip cases. In the free-slip cases, the spacing

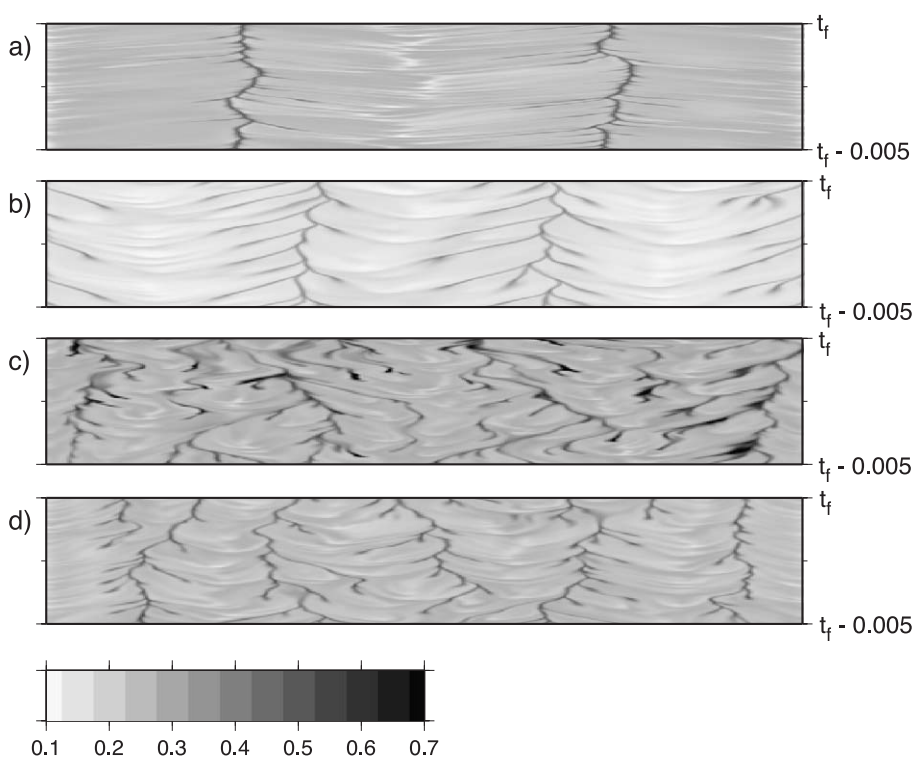


Fig. 3. Temperature versus time along the plume line. Time has been scaled according to Table 2. The time scale is identical for each plot, and only the final segment of time is shown. The effective Rayleigh number for all cases is 3.6×10^6 . (a) Isochemical, free-slip, (b) isochemical, no-slip, (c) thermochemical, $B=0.8$, viscosity equivalent in both components. (d) Thermochemical, $B=1.4$, viscosity equivalent in both components. The temperature scale is given at the bottom.

of downwellings and upwellings are similar where as in the no-slip cases, the spacing between upwellings is much smaller than that of downwellings. Comparing the low Rayleigh number cases shown in Fig. 1c,d it is observed that the free-slip calculation has three upwellings and three downwellings whereas the no-slip case has three downwellings and four upwellings. Therefore, more plumes are formed in the no-slip cases, but they migrate toward regions between the more widely spaced downwellings, resulting in greater horizontal plume motion (Fig. 1a,b). In addition, the reduced convective vigor imposed by the no-slip bottom boundary condition reduces the surface velocity, resulting in an even greater plume to surface velocity ratio (shown later).

Fig. 2 contains snapshots of both temperature and composition from thermochemical convection calculations which have similar effective Rayleigh numbers

in their top layers as the isochemical case shown in Fig. 1a,b. In this case, the viscosity of both chemical components is the same. The two calculations shown are for buoyancy numbers 1.4 (Fig. 2a,b) and 0.8 (Fig. 2c,d). The compositional fields reveal a relatively flat interface between layers for the higher buoyancy number (Fig. 2a) and an interface marked by significant topography for the lower buoyancy number (Fig. 2c). Convection occurs in both layers, and entrainment of material across the interface occurs. Entrainment is more pronounced in the lower buoyancy number case, as expected and observed in laboratory studies [20,31,32]. Fig. 3c,d shows temperature versus time for the final segment of time for the two calculations shown in Fig. 2 and the isochemical cases in Fig. 1a,b with equivalent effective Rayleigh number for free-slip (Fig. 3a) and no-slip (Fig. 3b) bottom boundary conditions. Here and in the remaining time versus

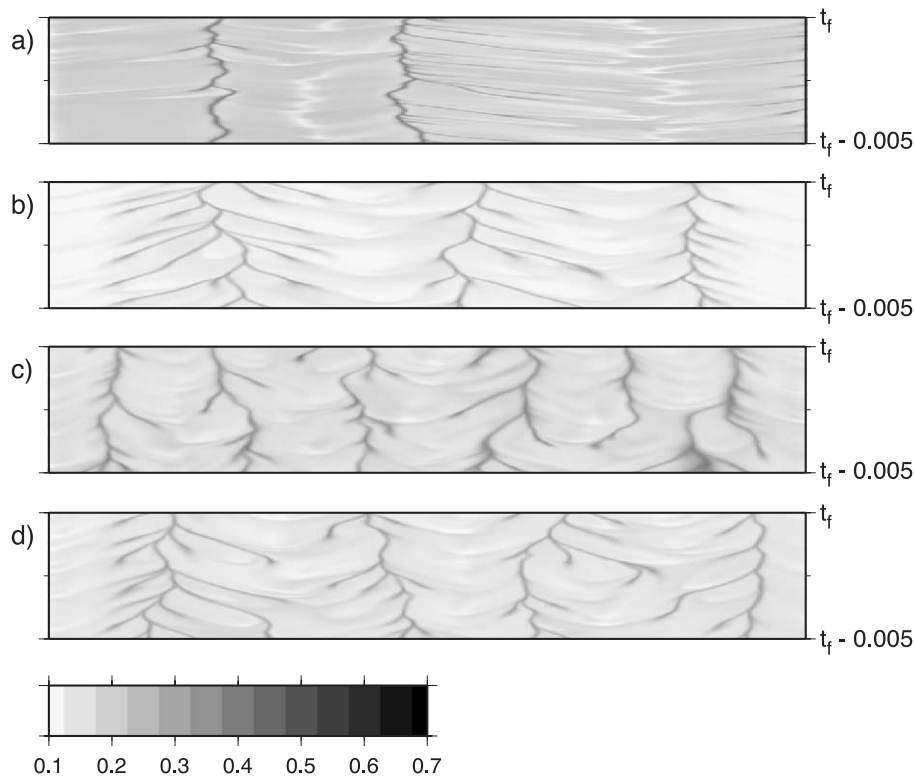


Fig. 4. Temperature versus time along the plume line. Time has been scaled according to Table 2. The time scale is identical for each plot, and only the final segment of time is shown. The effective Rayleigh number for all cases is 2.9×10^6 . (a) Isochemical, free-slip, (b) isochemical, no-slip, (c) thermochemical, $B=0.7$, (d) thermochemical, $B=1.0$. In both thermochemical calculations, the viscosity of the dense material is 25 times higher than the less dense material. The temperature scale is given at the bottom.

temperature figures, only a portion of the time evolution taken from the end of the calculation is shown. These time segments typically represent 5–10 transit times at the end of the calculation, and by visual inspection, we ensure that these time segments provide a proper representation of the entire time sequence.

The wide branches shown in the thermochemical calculations (Fig. 3c,d) and the no-slip isochemical calculation (Fig. 3b) reveal a smaller lateral spacing in plume development followed by significant horizontal motion. This behavior is not as pronounced in the free-slip isochemical case (Fig. 3a). By comparing these time series, it is evident that the presence of a dense component fails to stabilize the locations of plumes compared to isochemical convection of similar vigor. In fact, it may be argued that the free-slip isochemical case produces more stable plumes than both the no-slip isochemical case and the thermochemical cases. In

addition, the free-slip calculation leads to higher surface velocities than the no-slip isochemical and thermochemical cases, leading to even smaller plume surface velocity ratios as we will show later.

Fig. 4 shows the time evolution along the plume line for thermochemical calculations in which the more-dense component has an intrinsic viscosity increase of 25. In these two cases with buoyancy numbers 1.0 and 0.7, the increased viscosity on the dense component actually inhibits convection, leading to an effectively thickened lower thermal boundary layer resulting in a lower temperature drop across the top layer and weaker plumes generated at the interface. Again, the time evolution plots compare the thermochemical cases (Fig. 4c,d) with equivalent isochemical calculations (Fig. 4a,b), and they reveal that the thermochemical cases do not produce more stable plumes than the no-slip isochemical cases. In

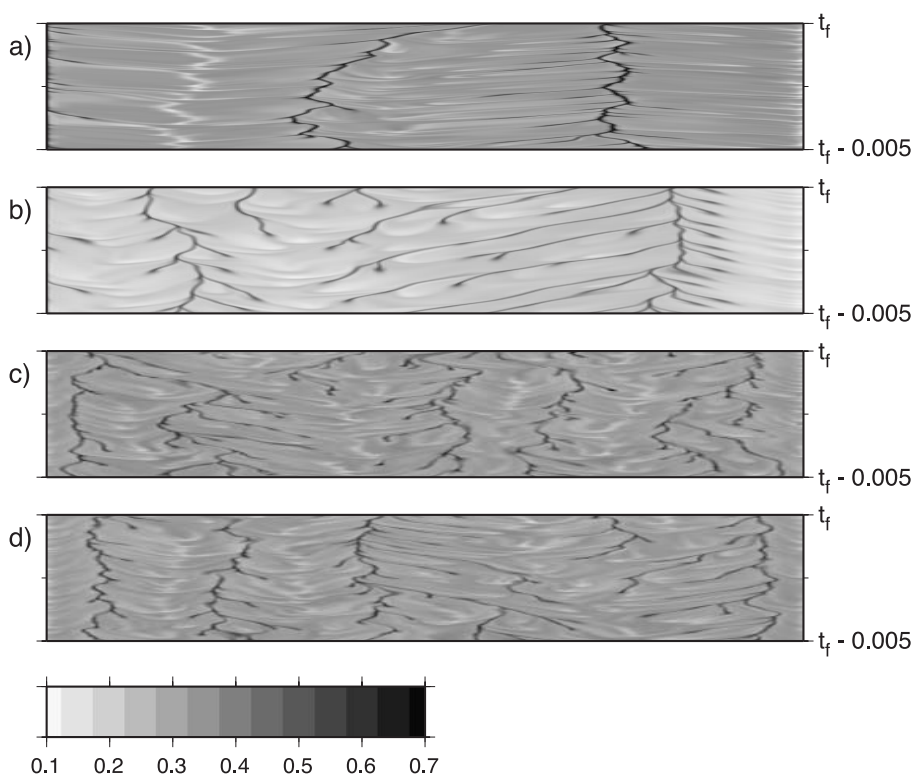


Fig. 5. Temperature versus time along the plume line. Time has been scaled according to Table 2. The time scale is identical for each plot, and only the final segment of time is shown. The effective Rayleigh number for all cases is 5.1×10^6 . (a) Isochemical, free-slip, (b) isochemical, no-slip, (c) thermochemical, $B=0.9$, (d) thermochemical, $B=1.2$. In both thermochemical calculations, the viscosity of the dense material is 25 times less than the less dense material. The temperature scale is given at the bottom.

addition, it appears that the free-slip isochemical case produces more stable plumes than the other cases.

Similar results are shown in Fig. 5 for thermochemical cases in which the more dense component has a viscosity reduction by a factor of 25. The weak dense layer convects vigorously, and there is significant entrainment of this material into the less dense layer. Again, the time evolution plots reveal a similar horizontal plume velocity for the thermochemical (Fig. 5c,d) and no-slip isochemical calculations (Fig. 5b), and it appears that the free-slip isochemical case (Fig. 5a) produces more stable plumes.

We performed one thermochemical convection calculation (both components have the same viscosity and the buoyancy number is 1.0) to compare to the lower Rayleigh number isochemical calculations shown in Fig. 1c,d. The time versus temperature plots for the two isochemical cases and the thermochemical case are shown in Fig. 6. From the plots, it is clear that the isochemical cases produce significantly more plume stability than the thermochemical case at this low Rayleigh number.

It is important to ensure that we have compared thermochemical calculations with isochemical cases

with similar vigor. We calculate the dimensional surface velocity of each case which we use as a measure of convective vigor (e.g., [38]). The surface velocities of the isochemical cases are indeed similar if not more than those of the thermochemical cases in which they were compared. The convective vigor of the thermochemical cases are more similar to the no-slip isochemical cases than that of the free-slip isochemical case of the same effective Rayleigh number (the free-slip cases have surface velocities about 1.8 higher than the no-slip and thermochemical cases).

Quantitative results of all 2-D calculations are shown in Fig. 7 where the plume velocity ratio is plotted against buoyancy number. For clarity, we have separated results into groups reflecting the different input Rayleigh numbers used in the thermochemical calculations. Each group contains three thermochemical sets, defined by the viscosity contrast between chemical components. Thermochemical results are depicted by circles, squares, and triangles representing cases in which the components have the same viscosity, the dense component is 25 time more viscous, and the dense component is 25 time less viscous, respec-

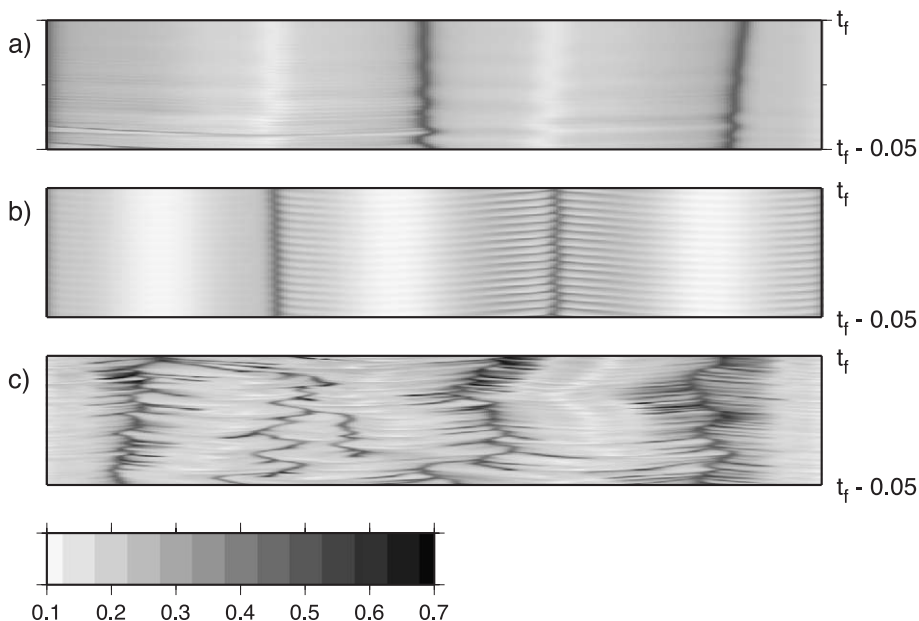


Fig. 6. Temperature versus time along the plume line. Time has been scaled according to Table 2. The time scale is identical for each plot, and only the final segment of time is shown. The effective Rayleigh number for all cases is 3.6×10^5 . (a) Isochemical, free-slip, (b) isochemical, no-slip, (c) thermochemical, $B=1.0$, viscosity equivalent in both components. The temperature scale is given at the bottom.

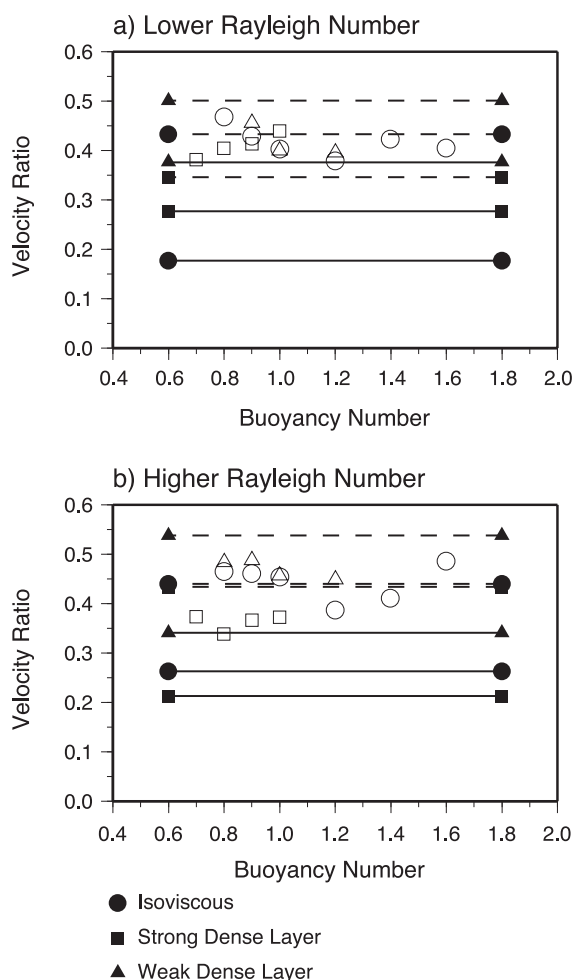


Fig. 7. Ratio of horizontal plume velocity to the average surface velocity plotted against buoyancy number for all calculations. For clarity, results are separated into two groups reflecting the Rayleigh numbers used for the thermochemical calculations: (a) 5×10^6 and (b) 10^7 . Thermochemical calculations are represented as circles, squares, and triangles for cases in which the dense material being equivalent to, 25 times more viscous, and 25 times less viscous than the less dense material, respectively. Solid and dashed lines represent results from free-slip and no-slip isochemical calculations, respectively. Filled symbols bounding each isochemical case line are used to indicate which thermochemical series that isochemical case should be compared to.

tively. Each set of thermochemical calculations is compared to two isochemical cases (six total) with free-slip (solid lines) and no-slip (dashed lines) bottom boundary conditions in which the thermochemical and isochemical cases have the same effective

Rayleigh number or convective vigor. Filled symbols bounding each line representing an isochemical case are used to identify which isochemical results a particular thermochemical set should be compared to. We find that the thermochemical results have plume velocity ratios similar to their respective isochemical cases with a no-slip bottom boundary condition. The results also show that the free-slip isochemical cases produce more stable plumes, with horizontal plume velocity to surface velocity ratios much lower than their respective thermochemical cases.

We performed two 3-D thermochemical calculations and the two 3-D isochemical calculations to compare to. The thermochemical calculations have a dense layer with viscosities that are the same as and 25 times less than the less dense material. Both isochemical cases have a free-slip bottom boundary condition. These cases are marked by asterisks in Table 1. Fig. 8(a,b) shows the +0.15 temperature residual for the isochemical and thermochemical case with a weak dense layer, respectively. The isochemical case produces a long-lived plume that migrates laterally near the position shown in Fig. 8a. The morphology of the dense layer in the thermochemical case is similar to that observed in [30] with circular embayments and linear ridges. We investigated the entire time series of the thermochemical calculation in which we observed a time-dependent topography along the interface. The location of embayments in this calculation is controlled by cold downwellings which push the dense material away. The time-dependent behavior of the downwellings in turn leads to a time-dependent interface topography. Plumes are much more closely spaced and migrate toward peaks along the density interface.

Fig. 8c,d shows +0.15 temperature residual along the plume plane as a function of time for the isochemical and thermochemical calculations, respectively. Both figures show the same span of dimensional time (vertical axis) which equates to approximately 5–10 transit times for the two cases. Unlike the 2-D cases, it is not visually apparent which case produces more fixed plumes. We plot the velocity ratio as a function of time for all four calculations in Fig. 8e,f. The isochemical and thermochemical velocity ratios are shown as black and gray curves, respectively. Fig. 8e and f shows results for the isoviscous comparison and

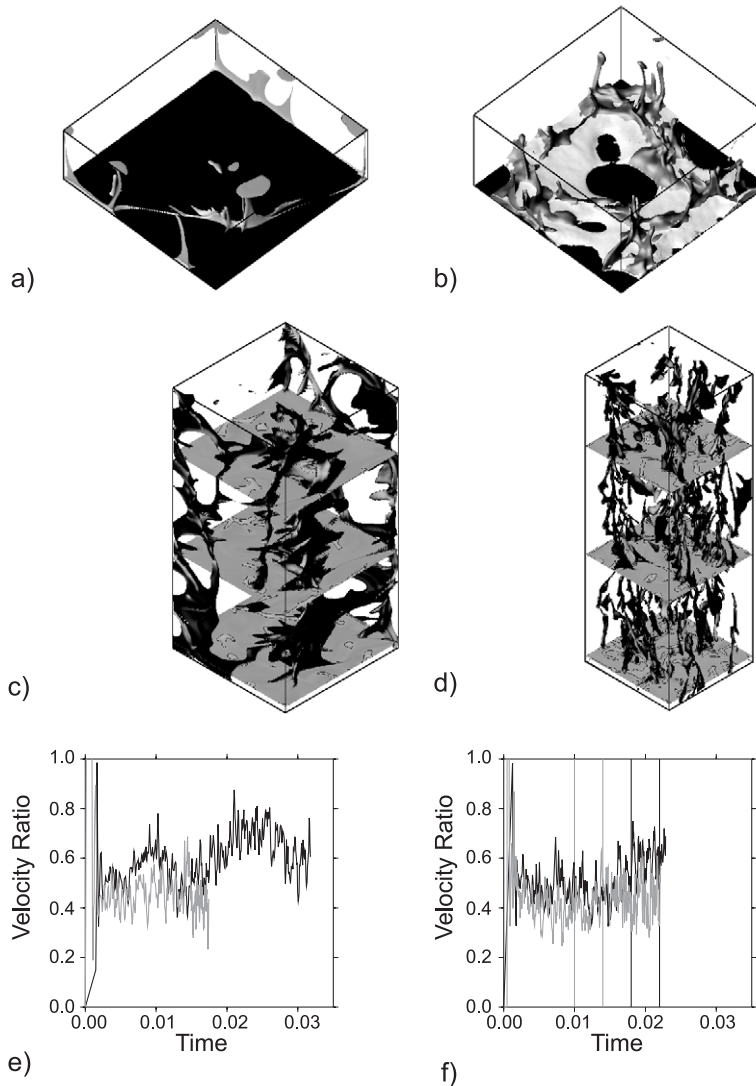


Fig. 8. Results from 3-D calculations comparing isochemical (a,c) and thermochemical (b,d) cases of comparable convective vigor. The dense layer is 25 times less viscous. (a,b) Residual temperature (0.15) isosurfaces of isochemical and thermochemical calculations. (c,d) Residual temperature isosurfaces versus time along the plume plane. Time is along the vertical axis. Planes displaying residual temperature along the plume plane are included to improve 3-D perspective. (e,f) The ratio of average horizontal plume velocity to average surface velocity versus time for both isochemical (black curves) and thermochemical (gray curves). Cases of comparable vigor for (e) an isoviscous rheology and a (f) 25 times less viscous dense layer. The gray (thermochemical) and black (isochemical) vertical lines in (f) are displayed to indicate the time windows used for the residual temperature versus time plots displayed in (c,d).

the cases with the weak dense layer comparison, respectively. The vertical black and gray lines in Fig. 8f represent the time windows used in Fig. 8c,d, respectively. We find that horizontal plume velocities tend to be about half of plate velocities for all cases shown. Unlike the 2-D results, there is

not a noticeable difference, either visually or quantitatively, in horizontal plume motion for the free-slip isochemical cases versus thermochemical cases. It is interesting to note from Fig. 8f that in the weak dense layer calculation (Fig. 8b,d), the dense material gets fully entrained at about time 0.016, followed by

whole mantle convection, yet the velocity ratio stays roughly the same, indicating no significant influence of thermochemical convection on the horizontal plume velocity to surface velocity ratio.

4. Discussion

By comparing horizontal plume velocities, both visually and quantitatively, between thermochemical and isochemical models of similar effective vigor we find that the presence of a dense layer fails to generate plumes which are more fixed than cases without a dense layer. In fact, we find that presence of a dense layer leads to convective behavior in the top layer similar to isochemical cases with no-slip bottom boundary conditions.

The presence of a dense layer provides a degree of viscous coupling, expected to be between no-slip and free-slip, and our results indicate that it is this coupling that most strongly influences the horizontal motion of plumes, not the presence of topography on a density interface. By comparing results from calculations with different buoyancy ratios, we find no striking difference in plume fixity between cases with a flat interface versus those with a large degree of topography (compare Figs. 3c with d, 4c with d, and 5c with d). However, we do notice that a higher topography often leads to the formation of longer-lived plumes along the peaks of the density interface.

By comparing isochemical calculations with free-slip and no-slip bottom boundary conditions, we find that the typical spacing of downwellings is similar. Upwellings, on the other hand, tend to be more closely spaced in the no-slip bottom boundary calculations than in the free-slip calculations which have an upwelling spacing more closely related to that of downwellings. This is in accordance to linear stability analysis (e.g., [38]). The free-slip calculations form a pattern of upwellings spaced between downwellings. No-slip calculations, however, produce plumes underneath as well as between downwellings which are swept aside laterally (Fig. 1b), leading to increased horizontal plume velocities. Examination of animations produced by these calculations reveal that the majority of these plumes actually form conduits that reach the surface as they migrate horizontally, so this

motion should be detected geologically. We propose that it is the incompatibility of upwelling and downwelling spacing that leads to a larger horizontal motion of plumes in no-slip isochemical and thermochemical models than in free-slip isochemical models.

Our results indicate that horizontal plume velocities are less than typical convective velocities, however, the presence of a dense layer does not lead to plumes more fixed than conventional isochemical convection. This is in contrast to conclusions drawn from laboratory experiments [20,30–32]. We do find, however, that when there is significant topography on the interface between chemical components, some long-lived plumes tend to be anchored to peaks on that interface, forming conduits of entrainment in agreement with laboratory studies. These peaks are mobile, dragging the attached plumes with them, forming what Davaille et al. [20] may consider as a “floating anchor.” For the viscosity contrasts applied in this study, the main control on the shape of interface for a given buoyancy ratio tends to be the downwellings which actively deform the interface. As a result of the time-dependent behavior of downwelling material, deformation along the density interface is equally time-dependent. In fact, it is difficult to envision a physical mechanism to maintain piles of dense material fixed in space while the less dense material is vigorously convecting. Peaks along the interface tend to migrate to regions between downwellings. More mobile plumes are typically formed off the peaks and are swept into the more-stable plumes on the peaks.

A possible reason for the difference in conclusions drawn from this study versus those from laboratory studies could be related to the distinction made between “thermals” (discrete blobs) and “plumes” (continuous upwellings) [30]. We make no distinction between the two, and we consider the fixity of plumes to be unrelated to whether the upwelling material takes the form of continuous long-lived conduits or short-lived upwellings that may be generated in the same location. If longevity of plumes is considered a prerequisite for fixity in laboratory experiments, perhaps different conclusions could be drawn, however, we do not think the geological and geophysical observations at and below hotspots complete enough to discern between a single long-lived and multiple short-lived upwellings. Another possible difference

could be related to the thermal strength of downwelling material. In our numerical experiments, active downwellings reach the dense layer interface, however, if laboratory experiments are carried out in a “stagnant lid” regime, then perhaps downwellings are weaker, reducing their ability to actively deform the dense layer.

Two aspects of this study that we consider to be important are (1) the comparison between thermochemical and isochemical models and (2) using the ratio of horizontal plume velocity to surface velocity. We find that in all calculations, both thermochemical and isochemical, horizontal plume velocities are significantly smaller than typical convective velocities. In order to test whether a dense component is actually responsible for plume fixity, it is crucial to compare between models with and without the dense component. Our understanding of convective vigor is primarily obtained by surface observables such as plate velocity and heat flow, so it is important to compare models with similar effective Rayleigh numbers of their top convecting layer. Because horizontal plume velocities increase with Rayleigh number, in order to test whether a dense layer can stabilize plumes, we must compare thermochemical calculations to isochemical convections with equivalent or slightly higher convective vigor. It would not suffice to simply investigate how plume velocity changes as the dense layer is fully entrained because the effective Rayleigh number of the top layer increases over a factor of 2 after the dense layer is removed. In addition, our notion of plume fixity is based on geological surface evidence, therefore, it is important to examine the ratio of horizontal plume velocity to surface velocity, although we must be careful to remember that the ratios we calculate are based on horizontal plume velocities near the source region and may not adequately reflect horizontal plume velocities at the surface. We note that the horizontal plume velocities are measured only a short vertical distance above their originating interface, and their horizontal motion at shallower depths tends to become more complicated. Our aim here is to study fixity of hotspots near the source region rather than at the surface of the mantle.

Some possible criticisms to this work are simplification of the model and entrainment issues. In order to keep this study simple and tractable, as done in laboratory studies, we have left out more complicated

features such as internal heating, temperature-dependent viscosity, the presence of large plates, depth-dependent thermodynamical properties, viscous heating, and adiabatic heating/cooling.

Although numerical models may effectively model the flow characteristics of a two-component system, there are difficulties accurately resolving entrainment (e.g., [16]). We believe that our tracer method has adequately captured the fundamental characteristic of entrainment, however, the exact degree may be somewhat different than that observed in laboratory measurements. We have performed a resolution test with finer grid resolution and a greater number of tracers and have found similar results.

To test the tracer method, we performed a resolution test for the 2-D thermochemical convection calculations with the highest effective Rayleigh number. In this case, the dense material is 25 times less viscous and the buoyancy number is 0.8. We doubled the amount of tracers to 32 per element (from 16). In addition, the element grid was refined to 96 and 576 vertical and horizontal elements, respectively (from 80×480). Visual inspection of the time versus temperature plots revealed no noticeable difference in character, and the quantitative measure of plume velocity to surface velocity was only 3% different between the two cases. We also found that surface heat flow and average convective velocities were similar. Overall, we found no significant difference between the two calculations, leading us to conclude that the resolution and density of tracers we used in this study are sufficient.

5. Conclusions

We compare both thermochemical and isochemical calculations with similar convective vigor in order to determine whether a dense component can enhance plume fixity. Our results indicate that horizontal plume velocities for thermochemical calculations are similar to those from isochemical calculations with no-slip bottom boundary conditions. In addition, we find that plumes tend to be more stable for isochemical calculations with free-slip bottom boundary conditions in two dimensions, however, this result is not evident in the limited number of three-dimensional calculations performed. In summary, we find that the

presence of a dense layer is not required to explain hotpot fixity. In fact, conventional isochemical convection produces equally or more fixed plumes.

Acknowledgements

We thank Paul Tackley, Michael Manga, and Mark Jellinek for careful and insightful reviews. This work is supported by the David and Lucile Packard Foundation and NSF under grant number EAR 0134939. *[SK]*

References

- [1] W.J. Morgan, Convection plumes in the lower mantle, *Nature* 230 (1971) 42.
- [2] P. Vogt, In the applicability of thermal conduction models to mid-plate volcanism: comments on a paper by Gaspis et al., *J. Geophys. Res.* 86 (1981) 950–960.
- [3] N.H. Sleep, Hotspots and mantle plumes: some phenomenology, *J. Geophys. Res.* 95 (1990) 6715–6736.
- [4] J. Ritsema, R.M. Allen, The elusive mantle plume, *Earth Planet. Sci. Lett.* 207 (2003) 1–12.
- [5] V. Courtillot, A. Davaille, J. Besse, J. Stock, Three distinct types of hotspots in the Earth's mantle, *Earth Planet. Sci. Lett.* 205 (2003) 295–308.
- [6] J.T. Wilson, A possible origin of the Hawaiian Island, *Can. J. Phys.* 41 (1963) 863–868.
- [7] P. Molnar, J. Stock, Relative motions of hotspots in the Pacific, Atlantic, and Indian Oceans since late Cretaceous time, *Nature* 327 (1987) 587–591.
- [8] R.A. Duncan, M.A. Richards, Hot spots, mantle plumes, flood basalts, and true polar wander, *Rev. Geophys.* 29 (1991) 31–50.
- [9] J.A. Tarduno, J. Gee, Large-scale motion between Pacific and Atlantic hotspots, *Nature* 378 (1995) 477–480.
- [10] T.H. Torsvik, R. Van der Voo, R.F. Redfield, Relative hotspot motions versus true polar wander, *Earth Planet. Sci. Lett.* 202 (2002) 185–200.
- [11] M.A. Richards, Hotspots and the case for a high viscosity lower mantle, in: R. Sabadini, K. Lambeck (Eds.), *Glacial Isostasy, Sea Level, and Mantle Rheology*, Kluwer Academic Publishing, Dordrecht, 1991, pp. 571–587.
- [12] B.M. Steinberger, R.J. O'Connell, Advection of plumes in mantle flow: implications for hotspots motion, mantle viscosity and plume distribution, *Geophys. J. Int.* 132 (1998) 412–434.
- [13] S. Zhong, M.T. Zuber, L. Moresi, M. Gurnis, Role of temperature-dependent viscosity and surface plates in spherical shell models of mantle convection, *J. Geophys. Res.* 105 (2000) 11063–11082.
- [14] J.P. Lowman, S.D. King, C.W. Gable, Steady plumes in viscously stratified, vigorously convecting, three-dimensional numerical mantle convection models with mobile plates, *Geochem. Geophys. Geosystems* 5 (2004) doi:10.1029/2003GC000583.
- [15] U.R. Christensen, A.W. Hofmann, Segregation of subducted oceanic crust in the convecting mantle, *J. Geophys. Res.* 99 (1994) 19867–19884.
- [16] P.J. Tackley, Three-dimensional simulations of mantle convection with a thermochemical CMB boundary layer: D''? in: M. Gurnis, M.E. Wyssession, E. Knittle, B.A. Buffett (Eds.), *The Core–Mantle Boundary Region*, Geodynamics Ser., vol. 28, AGU, Washington, DC, 1998, pp. 231–253.
- [17] L.H. Kellogg, B.H. Hager, R.D. van der Hilst, Compositional stratification in the deep mantle, *Science* 283 (1999) 1881–1884.
- [18] U. Hansen, D.A. Yuen, Extended-Boussinesq thermal–chemical convection with moving heat sources and variable viscosity, *Earth Planet. Sci. Lett.* 176 (2000) 401–411.
- [19] N.L. Montague, L.H. Kellogg, Numerical models of a dense layer at the base of the mantle and implications for the geodynamics at D'', *J. Geophys. Res.* 105 (2000) 11101–11114.
- [20] A. Davaille, F. Girard, M. Le Bars, How to anchor hotspots in a convecting mantle? *Earth Planet. Sci. Lett.* 203 (2002) 621–634.
- [21] A.W. Hofmann, Mantle geochemistry: the message from oceanic volcanism, *Nature* 385 (1997) 219–229.
- [22] M. Ishii, J. Tromp, Normal-mode and free-air gravity constraints on lateral variation in velocity and density of Earth's mantle, *Science* 285 (1999) 1231–1236.
- [23] R.D. van der Hilst, H. Karason, Compositional heterogeneity in the bottom 1000 kilometers of the Earth's mantle: toward a hybrid convection model, *Science* 283 (1999) 1885–1888.
- [24] G. Masters, G. Laske, H. Bolton, A. Dziewonski, The relative behavior of shear velocity, bulk sound speed, and compressional velocity in the mantle: implications for chemical and thermal structure, in: S. Karato, et al. (Eds.), *Earth's Deep Interior: Mineral Physics and Tomography from the Atomic to the Global Scale*, *Geophys. Monogr. Ser.* 117, (2000) 63–87.
- [25] L. Wen, P. Silver, D. James, R. Kuehnel, Seismic evidence for a thermo-chemical boundary at the base of the Earth's mantle, *Earth Planet. Sci. Lett.* 189 (2001) 141–153.
- [26] S. Ni, E. Tan, M. Gurnis, D. Helmberger, Sharp sides to the African superplume, *Science* 296 (2002) 1850–1852.
- [27] S. Ni, D.V. Helmberger, Ridge-like mantle structure beneath South Africa, *J. Geophys. Res.* 108 (2003) 2094.
- [28] S. Ni, D.V. Helmberger, Seismological constraints on the South African superplume; could be the oldest distinct structure on earth, *Earth Planet. Sci. Lett.* 206 (2003) 119–131.
- [29] A. Namika, K. Kurita, The influence of boundary heterogeneity in experimental models of mantle convection, *Geophys. Res. Lett.* 26 (1999) 1929–1932.
- [30] A.M. Jellinek, M. Manga, The influence of a chemical boundary layer on the fixity, spacing, and lifetime of mantle plumes, *Nature* 418 (2002) 760–763.
- [31] A. Davaille, Simultaneous generation of hotspots and super-

- swells by convection in a heterogenous planetary mantle, *Nature* 402 (1999) 756–760.
- [32] A. Davaille, M. Le Bars, C. Carbonne, Thermal convection in a heterogenous mantle, *C.r., Geosci.* 335 (2003) 141–156.
- [33] B. Romanowicz, Y. Gung, Superplumes from the core–mantle boundary to the lithosphere: implications for heat flux, *Science* 296 (2002) 513–516.
- [34] P.E. van Keken, S.D. King, H. Schmeling, U.R. Christensen, D. Neumeister, M.P. Doin, A comparison of methods for the modeling of thermochemical convection, *J. Geophys. Res.* 104 (1997) 22477–22496.
- [35] L. Moresi, M. Gurnis, Constraints on the lateral strength of slabs from three-dimensional dynamic flow models, *Earth Planet. Sci. Lett.* 138 (1996) 15–28.
- [36] P.J. Tackley, S.D. King, Testing the tracer ratio method for modeling active compositional fields in mantle convection simulations, *Geochem. Geophys. Geosystems* 4 (2003) doi: 10.1029/2001GC000214.
- [37] S. Zhong, B.H. Hager, Entrainment of a dense layer by thermal plumes, *Geophys. J. Int.* 154 (2003) 666–676.
- [38] G. Schubert, D.L. Turcotte, P. Olson, *Mantle convection in the Earth and planets*, Cambridge Univ. Press, Cambridge, 2001, 940 pp.